Cyclodextrin-induced suppression of PEG crystallization from the melt in a PEG-peptide conjugate

Hamley, I. W. ORCID: https://orcid.org/0000-0002-4549-0926, Castelletto, V., Hermida-Merino, D. and Rosenthal, M. (2024) Cyclodextrin-induced suppression of PEG crystallization from the melt in a PEG-peptide conjugate. ChemBioChem, 25 (19). e202400396. ISSN 1439-7633 doi: 10.1002/cbic.202400396

ChemBioChem

Research Article
doi.org/10.1002/cbic.202400396

Chemistry Europe
European Chemical Societies Publishing

www.chembiochem.org

Cyclodextrin-Induced Suppression of PEG Crystallization from the Melt in a PEG-Peptide Conjugate

Ian W. Hamley,*[a] Valeria Castelletto,[a] Daniel Hermida-Merino,[b] and Martin Rosenthal[b]

The influence of alpha-cyclodextrin (αCD) on PEG crystallization is examined for a peptide-PEG conjugate, YYKLVFF-PEG3k comprising an amyloid peptide YYKLVFF linked to PEG with molar mass 3 kg mol^{-1}. Remarkably, differential scanning calorimetry (DSC) and simultaneous synchrotron small-angle/wide-angle X-ray scattering (SAXS/WAXS) show that crystallization of PEG is suppressed by αCD, provided that the cyclodextrin content is sufficient. A hexagonal mesophase is formed instead. The αCD threading reduces the conformational flexibility of PEG, and hence suppresses crystallization. These results show that addition of cyclodextrins can be used to tune the crystallization of peptide-polymer conjugates and potentially other polymer/biomolecular hybrids.

Introduction

Within the field of supramolecular noncovalent chemistry, the control of host-guest interactions offers great scope in the development of novel supramolecular self-assembled materials.[1] Rotaxanes are model host-guest systems in which ring molecules thread around linear compounds. This class of complex includes simple bioderived compounds, as well as a diversity of molecules (often with more complex structures and functions for example use in molecular motors) that have been designed and developed over the last few decades.[2–5] An important class of biologically-derived compound that has been widely used as a model in host-guest chemistry is cyclodextrins, which comprise small rings of saccharide units (6, 7 and 8 in alpha-, beta- and gamma-cyclodextrin, αCD, βCD and γCD respectively) containing molecular-size cavities that can form inclusion complexes with polymers.[6] Cyclodextrins have a range of pharmaceutical applications since they can be used to create water-soluble complexes with hydrophobic drugs.[7–12] These simple cyclic carbohydrates are readily available commercially and have been shown to thread around different molecular chains including polymers and alkyl chains, depending on the size of the cyclodextrin ring (and hence cavity size) and its hydrophobicity/hydrophilicity. This can influence self-assembly due to the changes in molecular packing that result from inclusion complex formation, as demonstrated for example for surfactants[13–15] or copolymers such as those containing PEG,[16–20] among other systems. Among cyclodextrins, αCD contains six glucose-derived saccharides and contains a small hydrophobic cavity, which can thread around polymers including polyethylene glycol (PEG).[21–24]

Conjugation of poly(ethylene glycol), PEG, to peptides may be useful in therapeutic applications since PEG confers extended stability to peptide structures *in vivo* due to steric stabilization by PEG chains, as well as the increased mass which hinders rapid elimination from the body.[25–26] In addition, attachment of PEG which is hydrophilic to hydrophobic peptides produces amphiphilic molecules which can self-assemble into nanostructures such as fibrils, and at sufficiently high concentration liquid crystal structures. We have previously examined the self-assembly of PEG-peptides containing designed amyloid peptide fragments based on a core motif from the Amyloid β (Aβ), KLVFF (Aβ16–20)[27–30] in which the FF motif is believed to play an essential role in driving β-sheet formation through aromatic stacking interactions. We observed self-assembly into fibrils, and lyotropic liquid crystal phase formation at high concentration, including nematic and hexagonal columnar phases.[31–34] A further feature of the phase behavior of constructs containing PEG of sufficient molar mass is PEG crystallization in the solid state. We have examined this for KLVFF-PEG, AAKLVFF-PEG and FFKLVFF-PEG with PEG3k (i.e. polyethylene glycol with Mw = 3000 g mol^{-1}).[35–36] The latter two constructs contain dipeptide extensions of the core KLVFF peptide, respectively hydrophobic AA or hydrophobic and aromatic FF. We have also examined the effect of αCD on the crystallization of low molar mass PEG and found via a systematic study using differential scanning calorimetry (DSC) and SAXS/WAXS that sufficient αCD can suppress crystallization, leading instead to the formation of a hexagonal phase of αCD-wrapped PEG chains.[37]

We have recently established that αCD threading of PEG can change the self-assembled morphology of YYKLVFF-PEG3k in

[a] I. W. Hamley, V. Castelletto
School of Chemistry
Food Biosciences and Pharmacy
University of Reading
Whiteknights, Reading RG6 6AD, UK
E-mail: I.W.Hamley@reading.ac.uk

[b] D. Hermida-Merino, M. Rosenthal
DUBBLE-CRG @ ESRF
CS40220
The European Synchrotron
71, Avenue des Martyrs, 38043 Grenoble Cedex 9, France

Supporting information for this article is available on the WWW under https://doi.org/10.1002/cbic.202400396

aqueous solution.[38] We also quantified the extent of binding of αCD to the peptide-PEG conjugate by NMR analysis, and found saturated binding of 39 αCD molecules per PEG chain (which contain around 70 ethylene glycol repeat units). Here, we investigate the influence of αCD on the crystallization behaviour of YYKLVFF-PEG3k. DSC and simultaneous SAXS/WAXS were used to investigate the behaviour of dry samples, and heat/cool experiments reveal the unexpected suppression of PEG crystallization in complexes with sufficiently high αCD content and the formation of a hexagonal mesophase instead. These observations are rationalized based on the effect of αCD threaded onto PEG chains in restricting the conformational flexibility of the polymer.

Experimental

Materials. alpha-cyclodextrin (αCD) was obtained from Sigma-Aldrich (UK). The PEGylated conjugate YYKLVFF-PEG3k was synthesized by Rapp polymere GmbH using solid phase peptide synthesis methods. PEGylated TentaGel PAP resin was used, which comprises porous PS beads to which PEG is attached via acid cleavable linkages. The peptide was assembled from the C-terminus towards the N-terminus, and was attached to the solid support at the C-terminal via the α-carbonyl group of the amino acid. The crude peptide was characterized by reverse phase high performance liquid chromatography (RP-HPLC; Grom Saphir 200, C18 5 mm column). A mobile phase with a gradient of water with 0.1% TFA and acetonitrile with 0.75% TFA was used. Sample elution was monitored using a UV/vis detector operating at 220 nm. MALDI-TOF (Ultraflex, Bruker with matrix Universalmatrix, Fluka) was used to confirm $M_n = 4110\ g\,mol^{-1}$ for YYKLVFF-PEG3k, consistent with addition of YYKLVFF (Mn = 979.2 $g\,mol^{-1}$, expected) to the precursor PEG (Mn = 3139 $g\,mol^{-1}$, MALDI-TOF, 3060 $g\,mol^{-1}$ GPC). GPC (eluent: THF) of the starting PEG3k indicates Mw/Mn = 1.05.

To prepare the samples, convenient weighed amounts of αCD and water were placed in a vial. The αCD was dissolved using ultrasound and vortexing for 10 minutes. The transparent αCD solution was then used to dissolve a convenient weighed amount of YYKLVFF-PEG3k. As with the previous step, the YYKLVFF-PEG3k was dissolved using ultrasound and vortexing for another 10 minutes. The resulting αCD/YYKLVFF-PEG3k solution was allowed to rest for 24 hrs, and then dried on a glass slide for 24 hrs. The dried powder was recovered from the glass slide by scratching with a scalpel. Samples were then stored under vacuum before being studied by X-ray scattering or DSC.

Differential Scanning Calorimetry (DSC). Experiments were performed using a TA–Q200 DSC instrument. For the experiments, solutions were left to dry at room temperature on a microscope slide. After drying, the samples were recovered from the microscope slide surface using a scalpel, and the resulting powder was loaded in sealed DSC pans. An initial DSC experiment was carried out for for YYKLVFF-PEG3k using a T-ramp 19 °C→−40 °C→190 °C→−40 °C with a cool/heat rate of 10 °C/min. Subsequent temperature ramps were 19 °C→−40 °C→120 °C→−40 °C (ramp rate: 10 °C/min), because no significant changes were observed in the (120–190) °C range.

Simultaneous Small-Angle/Wide-Angle X-ray Scattering (SAXS/WAXS). Simultaneous SAXS/WAXS experiments were carried out on beamline DUBBLE (BM26)[39] at the ESRF (Grenoble, France) using an X-ray beam with a wavelength of 12 keV. The WAXS signal was acquired with a Pilatus 300 kw (1472×195 pixels) detector with a pixel size of 172 μm×172 μm whilst the SAXS signal was recorded with a Pilatus 1 M detector with 981×1043 pixels (172 μm×172 μm) at a sample-to-detector distance of 1.45 m. Alumina (α-Al_2O_3) was employed to calibrate the WAXS scattering angles and AgBe for the SAXS scattering angle range. The scattered intensity recorded in the area detectors was corrected by subtracting the empty DSC pan background by adjusting the X-ray sample transmission before being reduced to 1D intensity profiles as a function of the scattering vector ($q = 4\pi/\lambda\sin\theta$) using software bubble[40] The intensity is expressed in arbitrary units.

Results

Here we examine the influence of αCD on crystallization in complexes with the peptide-polymer conjugate YYKLVFF-PEG3k. Differential scanning calorimetry (DSC) was first used to identify phase transitions associated with PEG melting and crystallization. Figure 1 shows DSC thermograms obtained for YYKLVFF-PEG3k and co-assemblies with varying αCD content. The data for YYKLVFF-PEG3k alone in Figure 1a show a melting endotherm with peak at $T_m = 50.2$ °C and a crystallization exotherm at $T_c = 26.0$ °C on second cooling ramp. Upon incorporation of 0.1 wt% αCD, the melting endotherm and crystallization exotherm are retained (Figure 1b), although in the latter case there is greater undercooling (hysteresis) than for the conjugate alone, with the peak crystallization temperature $T_c = 18.5$ °C. The melting/crystallization peaks are greatly reduced but still present in the complexes with 1 wt% αCD (Figure 1c). Crystallization occurs with peak $T_c = 17$ °C. In contrast to these results, there is no evidence for PEG melting/crystallization peaks in the DSC data (Figure 1d,e) for samples containing 5 or 10 wt% αCD which, as for αCD itself (Figure 1f), just show a broad peak on heating due to water loss, starting at 70 °C. To complement DSC, TGA was used to confirm that no detectable degradation of YYKLVFF-PEG3k occurs below 250 °C (SI Figure S1).

Simultaneous synchrotron SAXS/WAXS was used to further elucidate structural aspects of PEG crystallization in YYKLVFF-PEG3k/αCD blends in the dry state (and its suppression at high αCD content). Figure 2 shows simultaneous SAXS/WAXS data for YYKLVFF-PEG3k in the absence of αCD. The WAXS data (Figure 2a) shows the disappearance of PEG crystal reflections on heating and their reversible reappearance on cooling, and re-melting on second heating (the temperature profile is shown in Figure 2c). The WAXS data for the crystalline PEG (Figure 2d) were indexed using the published unit cell data for PEG (SI Figure S2a),[41] as described earlier in our study on KLVFF-PEG3k, AAKLVFF-PEG3k and FFKLVFF-PEG3k.[35] The SAXS data in Figure 2b shows reversible changes in the scattering around $q = 0.8–0.85\ nm^{-1}$ which is associated with the presence of a peak (correlation hole peak[42–43]) in the melt state which is suppressed upon PEG crystallization as evident from the selected frames shown in Figure 2e. A peak in the SAXS profile in the melt state was previously reported for the KLVFF-PEG3k conjugates.[36] Similar behaviour, i.e. WAXS peaks for crystalline PEG and reversible melting/crystallization was observed for the blend with low αCD content (0.1 wt%) as shown in SI Figure S3.

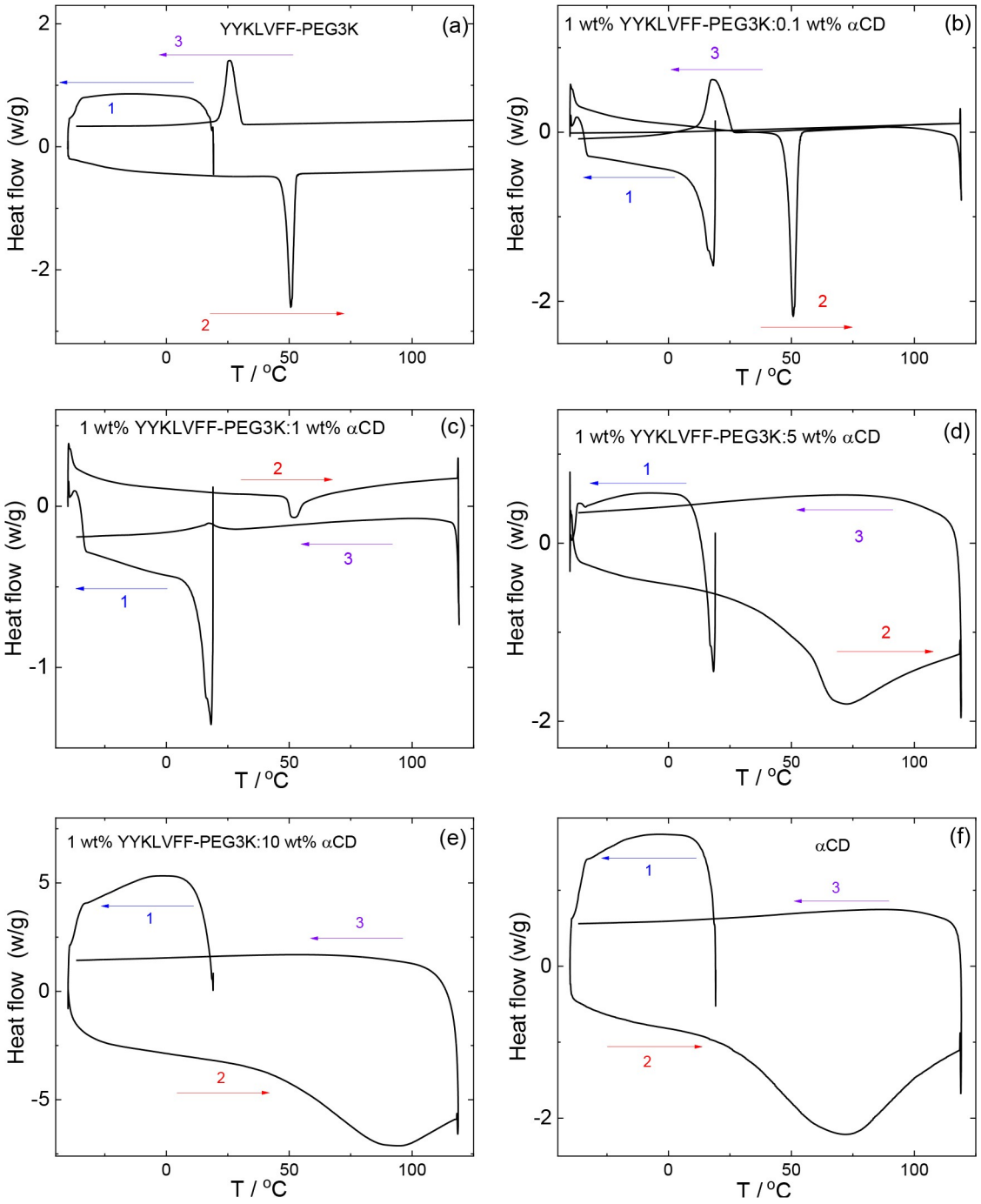

Figure 1. DSC data measured for 1 wt% YYKLVFF-PEG3k with (a) 0, (b) 0.1, (c) 1, (d) 5 and (10) 10 wt% αCD. (f) αCD. The arrows point to the direction of the changes in T: (1) is the first cooling ramp from room temperature to −40 °C, (2) is the first heating ramp from −40 to 120 °C and (3) is the second cooling ramp from 120 °C to −40 °C.

The simultaneous SAXS/WAXS data in Figure 3 show completely different behavior for the YYKLVFF-PEG3k/αCD blend containing 10 wt% αCD. There are no PEG crystal diffraction peaks (Figure 3 a,d) and no changes in the SAXS profiles (Figure 3c,d) which retain a broad peak around $q = 0.8\ nm^{-1}$. The WAXS data shows a sharp peak at $q = 14.2\ nm^{-1}$ ($d = 0.45$ nm) as well as a number of weaker peaks, all in different positions to those observed for PEG (cf. SI Figure S2a) and so these are ascribed to the formation of complexes of αCD with PEG (with a main spacing $d = 0.45$ nm) which is unable to crystallize when wrapped with αCD molecules. In support of this assignment, the strong peak at $q = 14.2\ nm^{-1}$ is close to features in the WAXS profile for αCD itself (Figure S2b). Similar behavior is observed for the other blend with higher αCD content (5 wt%) as shown in SI Figure S4. The blend with 1 wt% αCD shows some aspects of PEG crystallization/melting as shown in SI Figure S5 where the WAXS shows peak changes for first melting. However the pattern is dominated by the $q =$

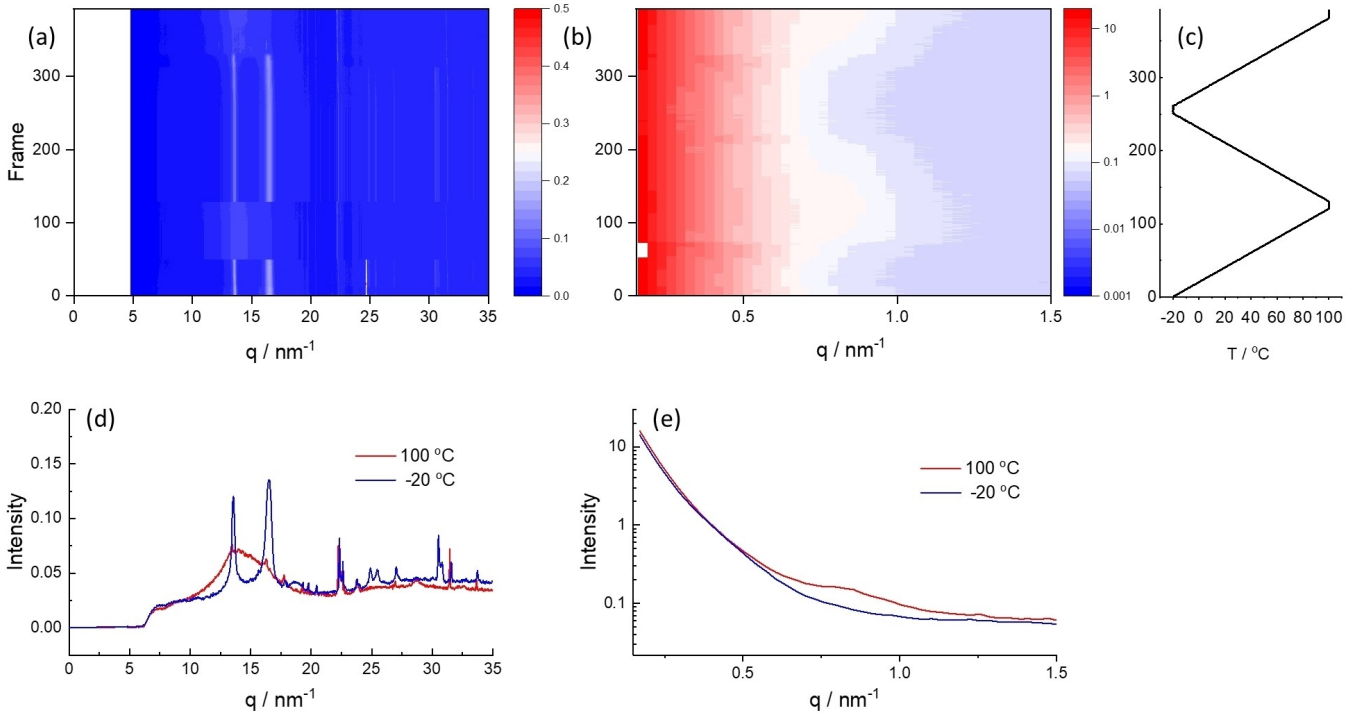

Figure 2. SAXS/WAXS data for YYKLVFF-PEG3k during a heat/cool/heat cycle at 5 °C/min (a) WAXS data heatmap, (b) SAXS data heatmap (intensity for each frame stacked vertically), (c) Temperature ramp profile corresponding to the heatmaps in (a,b), (d) Selected frames of WAXS data at the temperatures indicated (from first heat/first cool), Selected frames of SAXS data at the temperatures indicated (from first heat/second cool).

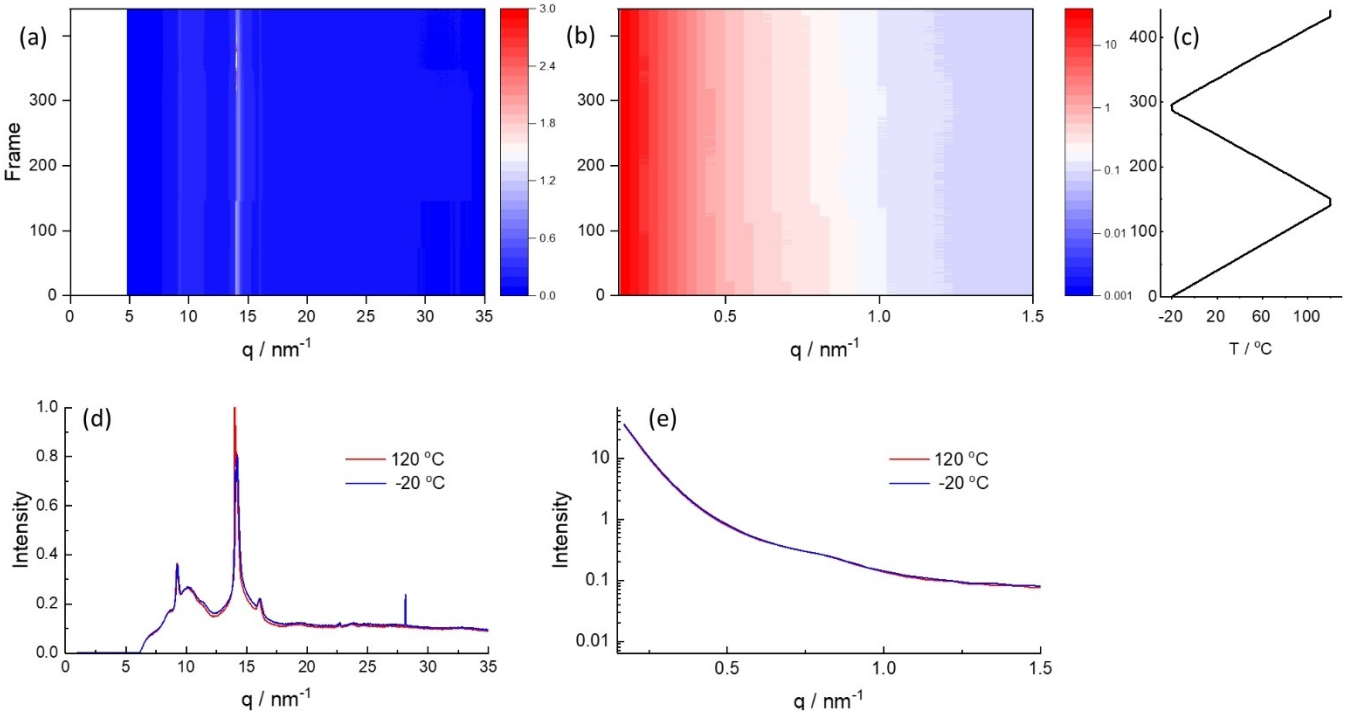

Figure 3. SAXS/WAXS data for YYKLVFF-PEG3k/10 wt% αCD blend during a heat/cool/heat cycle at 5 °C/min (a) WAXS data heatmap, (b) SAXS data heatmap (intensity for each frame stacked vertically), (c) Temperature ramp profile corresponding to the heatmaps in (a,b), (d) Selected frames of WAXS data at the temperatures indicated (from first heat/first cool), Selected frames of SAXS data at the temperatures indicated (from first heat/second cool).

14.2 nm^{-1} peak as observed for the other high αCD blends, and there are only small changes in the SAXS profiles.

The reversibility of PEG melting and cooling is shown in the SAXS/WAXS data for the mixture with 0.1 wt% αCD (SI Fig-

ure S3). This shows the high degree of reversibility of these transitions following second heating and cooling and third heat/cool cycles.

The SAXS data at high q (SI Figure S6 shows selected frames) reveals additional peaks for the blends containing high αCD content, in particular there are well-defined first order peak at $q = 5.36\ nm^{-1}$, $q = 5.38\ nm^{-1}$, or $q = 5.40\ nm^{-1}$, for blends containing 1, 5 or 10 wt% αCD, respectively. This peak is present over the full temperature range, but with reduced intensity at high temperature (and shifted to slightly lower q). The peak is absent for αCD alone (SI Figure S6) therefore it is due to complexation of αCD with PEG and the corresponding spacings $d = 1.172$ nm, $d = 1.168$ and $d = 1.164$ for mixtures with 1, 5 or 10 wt% αCD show a reduction in periodicity with increase in αCD content, reflecting a more compact complexed structure. The combination of SAXS and WAXS in fact provides unique insight into the unexpected non-crystalline ordering in the complexes at high αCD content. The data is shown in Figure 4 which shows a series of reflections for all three high αCD blends that can be indexed to a hexagonal lattice structure with reflections at q^*, $\sqrt{3}q^*$, $\sqrt{7}q^*$ and 3 q^*. The $\sqrt{7}q^*$ peak at $q = 14.2\ nm^{-1}$ is enhanced because it is close to the peak at $q = 14.1\ nm^{-1}$ for αCD itself (Figure S2b), this corresponds to the αCD inner diameter.[44] The expected reflection at $2q^*$ is absent to the degeneracy in hexagonal lattice orientation (0° and 30° rotation). It is believed that the additional broad peaks in Figure 4 and SI Figure S6 near $q = 3.8\ nm^{-1}$ (for the 1 wt% αCD and 5 wt% αCD blends) or $q = 4.0\ nm^{-1}$ for the 10 wt% αCD blend are due to the presence of amorphous structure (PEG not wrapped by αCD). The hexagonal lattice has a lattice parameter $d_{hex} = 1.353$–1.344 nm for blends with 1–10 wt% αCD from the hexagonal lattice spacings $d = d_{10}$. This is close to the estimated outer diameter of an αCD ring[44] and this illustrates close-packing of αCD-wrapped PEG chains in the hexagonal inclusion complexes.

Thus, both the SAXS/WAXS data and the DSC data show that PEG crystallization occurs in YYKLVFF-PEG3 K and blends with low αCD content (0 or 0.1 wt%) but it is entirely suppressed in blends containing higher αCD content, where a hexagonal phase of close-packed αCD-wrapped PEG chains is formed instead, as illustrated in Figure 5.

Discussion and Conclusions

Complex formation between PEG1k and αCD leading to a channel-like crystal structure of αCD-threaded PEG chains was reported in 1990.[21] The XRD data show many sharp Bragg peaks characteristic of a highly crystalline material, in contrast to our WAXS data which shows semi-crystalline features. Also in complete contrast to our findings, it has previously been reported that addition of non-stoichiometric amounts of αCD to polymers, which causes complex formation, can enhance crystallization from the melt (i.e. the αCD acts as nucleating agent),[45] as exemplified by reports on poly(3-hydroxybutyrate)[46–47] and on inclusion complexes of αCD with poly(ε-caprolactone), poly(butylene succinate) and PEG ($M_w = 20000\ g\,mol^{-1}$).[48–49]

Here, in YYKLVFF-PEG3k, the suppression of PEG crystallization is due to inclusion complex formation, i.e. wrapping by

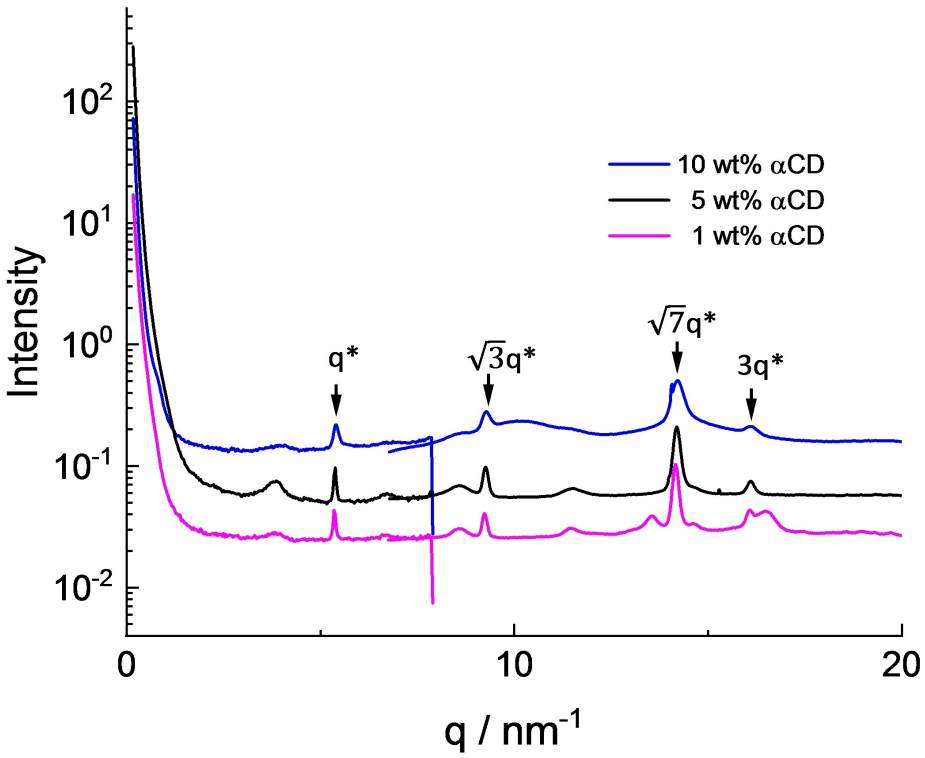

Figure 4. Combined SAXS/WAXS for complexes with high αCD content (indicated). The WAXS data have been scaled by arbitrary factors to overlap SAXS data.

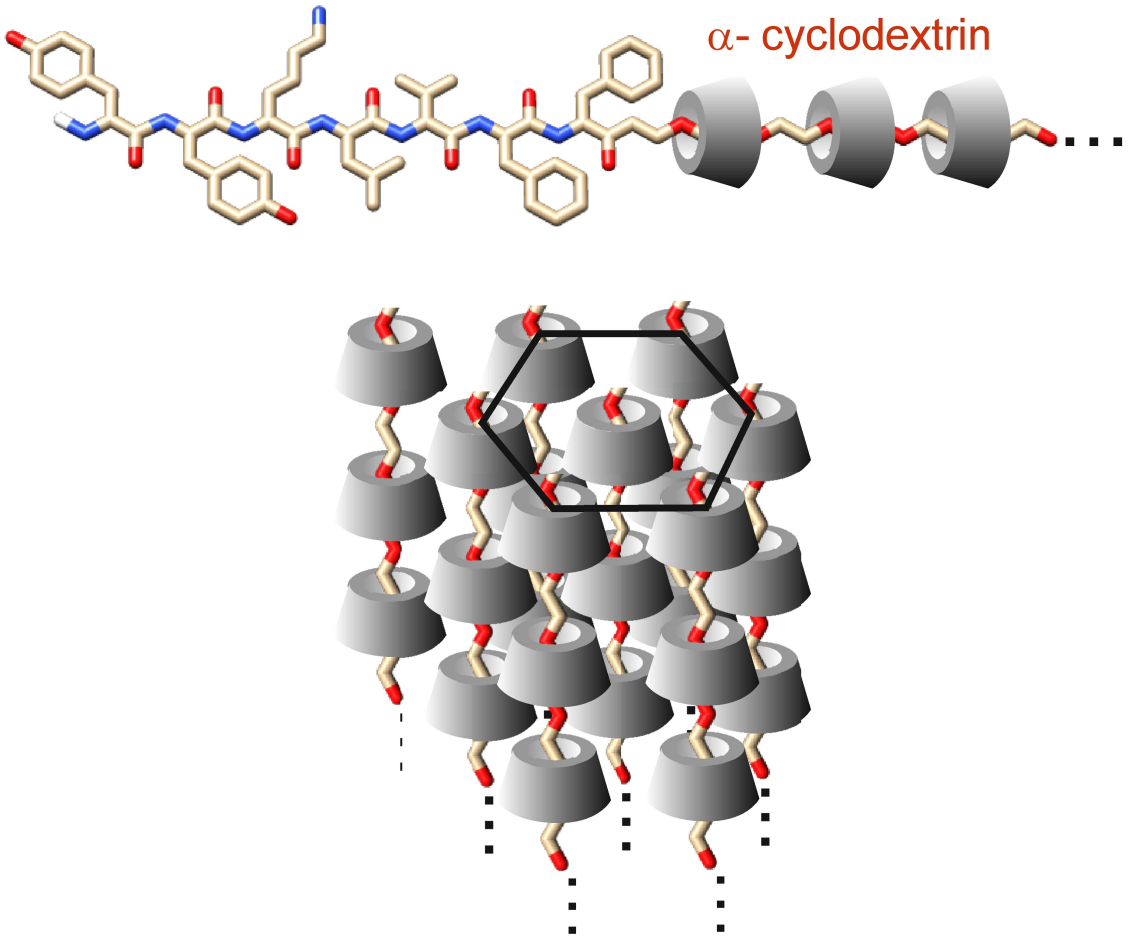

Figure 5. Scheme showing αCD wrapping PEG in complexes forming a hexagonal lattice.

αCD around PEG chains in blends at sufficiently high content. This presumably leads to greatly restricted conformational freedom, thus preventing PEG adopting the extended helical structure characteristic of the crystal state,[41] but instead the αCD-threaded PEG forms a hexagonal mesophase. The formation of a hexagonal phase by αCD-wrapping of PEG was reported by Topchieva *et al.* on the basis of WAXS (XRD),[50] and more recently we confirmed this finding and also examined the suppression of PEG crystallization (and the formation of a hexagonal mesophase) as a function of αCD content in blends with PEG1k, PEG3k and PEG6k.[37] Here, this phenomenon is demonstrated to occur also in peptide-PEG conjugates, i.e. the peptide end group does not affect the αCD-wrapping of PEG in this case. Compared to the combined SAXS/WAXS data for the PEG homopolymers in our recent paper, the data in Figure 4 in fact show a cleaner signature of a hexagonal phase. The peaks in the data are due to the hexagonal lattice and there are no additional peaks due to the stacking of αCD along the PEG chains, in contrast to the data for the low molar mass PEG homopolymers.[37] This suggests that the YYKLVFF peptide "end groups" may influence the threading of the αCD chains on the PEG chains, and this is less ordered in the YYKLVFF-PEG3k conjugate than the corresponding PEG3k polymer (or PEG1k or PEG6k polymer).[37] An alternative explanation for this might be based on differences in the polydispersity of the PEG in the YYKLVFF-PEG3k conjugate compared to the low molar mass PEG polymers, which in turn might influence the extent of PEG threading, however the PEG3k in YYKLVFF-PEGk is of low dispersity ($Đ = 1.05$) as are the PEG samples in our recent study so this does not seem to be the most probable explanation for the difference, which we rather assign to an end group effect. It will be interesting in future work to examine the effect of peptide length on the crystallization of low molar mass PEG. In our previous studies on KLVFF-PEG3k, AAKLVFF-PEG3k and FFKLVFF-PEG3k we observed an interplay between amyloid β-sheet formation by the peptide and PEG crystallization.[35–36] Signatures of cross-β peptide structure (in XRD patterns) were disrupted by PEG crystallization for the weak fibrillizer KLVFF, whereas peptide fibrils are retained for the conjugates containing the stronger fibrillizers AAKLVFF and FFKLVFF. In this case it is probable that the peptide fibrillization tendency (which depends on the number of hydrophobic and aromatic residues) influences the balance between crystallization and peptide ordering, not just the peptide length. Clearly, αCD also has a major impact on crystallization propensity due to its PEG-molar mass dependent formation of inclusion complexes.

In summary, our findings point to the generality of cyclodextrin-induced suppression of crystallization in PEG-containing

molecules and also show how αCD can be used to control the solid state morphology of polymer-peptide conjugates. This complements our study showing a change of nanostructure in aqueous solutions of YYKLVFF-PEG3k due to αCD host-guest complex formation.[38]

Acknowledgements

This work was supported by EPSRC Fellowship grant (reference EP/V053396/1) to IWH. We thank the ESRF for beamtime on BM29 (ref. MX-2513). We acknowledge use of facilities in the Chemical Analysis Facility (CAF) at the University of Reading.

Conflict of Interests

The authors declare no conflict of interest.

Data Availability Statement

The data that support the findings of this study are available from the corresponding author upon reasonable request.

Keywords: Peptide conjugate · PEG · SAXS/WAXS · Cyclodextrin

[1] T. Aida, E. W. Meijer, S. I. Stupp, *Science* **2012**, *335*, 813–817.
[2] R. A. Bissell, E. Cordova, A. E. Kaifer, J. F. Stoddart, *Nature* **1994**, *369*, 133–137.
[3] J. P. Collin, C. Dietrich-Buchecker, P. Gaviña, M. C. Jimenez-Molero, J. P. Sauvage, *Acc. Chem. Res.* **2001**, *34*, 477–487.
[4] K. Kim, *Chem. Soc. Rev.* **2002**, *31*, 96–107.
[5] J. Berná, D. A. Leigh, M. Lubomska, S. M. Mendoza, E. M. Pérez, P. Rudolf, G. Teobaldi, F. Zerbetto, *Nat. Mater.* **2005**, *4*, 704–710.
[6] G. Wenz, B. H. Han, A. Muller, *Chem. Rev.* **2006**, *106*, 782–817.
[7] T. Loftsson, M. E. Brewster, *J. Pharm. Sci.* **1996**, *85*, 1017–1025.
[8] K. Uekama, F. Hirayama, T. Irie, *Chem. Rev.* **1998**, *98*, 2045–2076.
[9] M. E. Davis, M. E. Brewster, *Nat. Rev. Drug Discovery* **2004**, *3*, 1023–1035.
[10] E. M. M. Del Valle, *Process Biochem.* **2004**, *39*, 1033–1046.
[11] M. E. Brewster, T. Loftsson, *Adv. Drug Delivery Rev.* **2007**, *59*, 645–666.
[12] T. Loftsson, D. Duchene, *Int. J. Pharm.* **2007**, *329*, 1–11.
[13] L. X. Jiang, Y. Peng, Y. Yan, M. L. Deng, Y. L. Wang, J. B. Huang, *Soft Matter* **2010**, *6*, 1731–1736.
[14] C. C. Tsai, W. B. Zhang, C. L. Wang, R. M. Van Horn, M. J. Graham, J. Huang, Y. M. Chen, M. M. Guo, S. Z. D. Cheng, *J. Chem. Phys.* **2010**, *132*.
[15] L. D. S. Araujo, L. Watson, D. A. K. Traore, G. Lazzara, L. Chiappisi, *Soft Matter* **2022**, *18*.
[16] J. Li, X. P. Ni, Z. H. Zhou, K. W. Leong, *J. Am. Chem. Soc.* **2003**, *125*, 1788–1795.
[17] E. Larraneta, J. R. Isasi, *Langmuir* **2012**, *28*, 12457–12462.
[18] C. Stoffelen, J. Huskens, *Small* **2016**, *12*, 96–119.
[19] A. Dominski, T. Konieczny, P. Kurcok, *Materials* **2020**, *13*.
[20] J. Choi, H. Ajiro, *Soft Matter* **2022**, *18*, 8885–8893.
[21] A. Harada, M. Kamachi, *Macromolecules* **1990**, *23*, 2821–2823.
[22] A. Harada, J. Li, M. Kamachi, *Nature* **1992**, *356*, 325–327.
[23] S. Yamada, Y. Sanada, A. Tamura, N. Yui, K. Sakurai, *Polym. J.* **2015**, *47*, 464–467.
[24] S. Uenuma, R. Maeda, H. Yokoyama, K. Ito, *Macromolecules* **2019**, *52*, 3881–3887.
[25] I. W. Hamley, *Biomacromolecules* **2014**, *15*, 1543–1559.
[26] H. Acar, J. M. Ting, S. Srivastava, J. L. LaBelle, M. V. Tirrell, *Chem. Soc. Rev.* **2017**, *46*, 6553–6569.
[27] L. O. Tjernberg, C. Lilliehook, D. J. E. Callaway, J. Naslund, S. Hahne, J. Thyberg, L. Terenius, C. Nordstedt, *J. Biol. Chem.* **1997**, *272*, 17894–17894.
[28] L. O. Tjernberg, D. J. E. Callaway, A. Tjernberg, S. Hahne, C. Lilliehöök, L. Terenius, J. Thyberg, C. Nordstedt, *J. Biol. Chem.* **1999**, *274*, 12619–12625.
[29] M. J. Krysmann, V. Castelletto, A. Kelarakis, I. W. Hamley, R. A. Hule, D. J. Pochan, *Biochemistry* **2008**, *47*, 4597–4605.
[30] I. W. Hamley *Chem. Rev.* **2012**, *112*, 5147–5192.
[31] I. W. Hamley, M. J. Krysmann, V. Castelletto, L. Noirez, *Adv. Mater.* **2008**, *20*, 4394–4397.
[32] I. W. Hamley, M. J. Krysmann, V. Castelletto, A. Kelarakis, L. Noirez, R. A. Hule, D. Pochan, *Chem. Eur. J.* **2008**, *14*, 11369–11374.
[33] V. Castelletto, G. E. Newby, Z. Zhu, I. W. Hamley, L. Noirez, *Langmuir* **2010**, *26*, 9986–9996.
[34] V. Castelletto, G. E. Newby, D. Hermida-Merino, I. W. Hamley, D. Liu, L. Noirez, *Polym. Chem.* **2010**, *1*, 453–459.
[35] I. W. Hamley, M. J. Krysmann, *Langmuir* **2008**, *24*, 8210–8214.
[36] M. J. Krysmann, S. S. Funari, E. Canetta, I. W. Hamley *Macromol. Chem. Phys.* **2008**, *209*, 883–889.
[37] I. W. Hamley, V. Castelletto, *ACS Polymers Au* **2024**, in press.
[38] V. Castelletto, R. M. Kowalczyk, J. Seitsonen, I. W. Hamley, *ChemBioChem* **2023**, e202300472.
[39] G. Portale, D. Cavallo, G. C. Alfonso, D. Hermida-Merino, M. van Drongelen, L. Balzano, G. W. M. Peters, J. G. P. Goossens, W. Bras, *J. Appl. Crystallogr.* **2013**, *46*, 1681–1689.
[40] V. Dyadkin, P. Pattison, V. Dmitriev, D. Chernyshov, *J. Synchrotron Radiat.* **2016**, *23*, 825–829.
[41] Y. Takahashi, H. Tadokoro, *Macromolecules* **1973**, *6*, 672–675.
[42] P. G. de Gennes, *Scaling Concepts in Polymer Physics*, Cornell University Press, Ithaca, **1979**.
[43] I. W. Hamley, *The Physics of Block Copolymers*, Oxford University Press, Oxford, **1998**.
[44] L. Huang, A. E. Tonelli, *Journal of Macromolecular Science-Reviews in Macromolecular Chemistry and Physics* **1998**, *C38*, 781–837.
[45] A. E. Tonelli, in *Inclusion Polymers, Vol. 222* (Ed.: G. Wenz), **2009**, pp. 115–166.
[46] Y. He, Y. Inoue, *Biomacromolecules* **2003**, *4*, 1865–1867.
[47] R. Vogel, B. Tandler, L. Haussler, D. Jehnichen, H. Brunig, *Macromol. Biosci.* **2006**, *6*, 730–736.
[48] T. Dong, Y. He, B. Zhu, K. M. Shin, Y. Inoue, *Macromolecules* **2005**, *38*, 7736–7744.
[49] T. Dong, K. M. Shin, B. Zhu, Y. Inoue, *Macromolecules* **2006**, *39*, 2427–2428.
[50] I. N. Topchieva, A. E. Tonelli, I. G. Panova, E. V. Matuchina, F. A. Kalashnikov, V. I. Gerasimov, C. C. Rusa, M. Rusa, M. A. Hunt, *Langmuir* **2004**, *20*, 9036–9043.

Manuscript received: April 30, 2024
Revised manuscript received: May 17, 2024
Accepted manuscript online: May 22, 2024
Version of record online: June 28, 2024